Measurement of the iron spectrum with CALET on the International Space Station

Francesco Stolzi,[a,b,*] **Caterina Checchia**[a] **and Yosui Akaike**[c,d] **on behalf of the CALET Collaboration**
(a complete list of authors can be found at the end of the proceedings)

[a]*Department of Physical Sciences, Earth and Environment,*
University of Siena, via Roma 56, 53100 Siena, Italy

[b]*INFN Sezione di Pisa,*
Polo Fibonacci, Largo B. Pontecorvo, 3, 56127 Pisa, Italy

[c]*Waseda Research Institute for Science and Engineering,*
Waseda University, 17 Kikuicho, Shinjuku, Tokyo 162-0044, Japan

[d]*JEM Utilization Center, Human Spaceflight Technology Directorat, Japan Aerospace Exploration Agency,*
2-1-1 Sengen, Tsukuba, Ibaraki 305-8505, Japan
E-mail: francesco.stolzi@unisi.it, caterina.checchia2@unisi.it, yakaike@aoni.waseda.jp

The Calorimetric Electron Telescope (CALET), in operation on the International Space Station since 2015, has collected a large sample of cosmic-ray charged particles and gamma-rays over a wide energy interval. The instrument consists of two layers of segmented plastic scintillators to identify the charge of individual elements from proton to iron (and above), a thin imaging tungsten scintillating fiber calorimeter providing accurate particle tracking, and a lead-tungstate homogeneous calorimeter to measure energy. One of the scientific objectives of CALET is the direct measurement of the energy spectra of cosmic nuclei conveying important information on their acceleration and propagation in the Galaxy. Based on the first five years of CALET observation, CALET has measured the iron spectrum in the range of kinetic energy per nucleon from 10 GeV/n to 2.0 TeV/n. We present the CALET iron results, describe the analysis of the data and the detailed assessment of systematic uncertainties, and compare the CALET results with the findings of previous experiments.

---

*Presenter

1. Introduction

Direct measurements of charged cosmic rays (CR) have revealed unexpected spectral features such as a hardening in the proton, helium [1–7] and heavy nuclei spectra around a few hundred GeV/n [8–12]. In order to discriminate among several classes of theoretical models proposed to explain these spectral structures [13–19] a precision measurement of the iron spectrum is of particular interest, as iron provides favorable conditions for observations due to its largest relative abundance among the heavy elements and also for a negligible contamination from spallation of higher mass elements.

The CALorimetric Electron Telescope (CALET) [20–22], a space-based instrument optimized for the measurement of the all-electron spectrum [23, 24], reported results of the proton spectrum up to 10 TeV [7] and, recently, of carbon and oxygen nuclei to 2.2 TeV/n [12]. Thanks to its large dynamic range, adequate calorimetric depth, accurate tracking, and excellent charge identification capabilities, CALET is carrying out extensive measurements of individual chemical elements in CR up to iron and above in the energy range from few GeV up to 1 PeV. In this paper, we describe the analysis procedure for iron flux measurement and present the energy spectra from 10 GeV/n to 2.0 TeV/n, based on the data collected by CALET from January 1, 2016 to May 31, 2020 aboard the International Space Station (ISS).

2. CALET instrument

CALET is an all-calorimetric instrument consisting of a pair of plastic scintillator hodoscopes acting as CHarge Detector (CHD), a finely segmented pre-shower IMaging Calorimeter (IMC), and a Total AbSorption Calorimeter (TASC). CALET measures the particle energy with the TASC, a lead-tungstate homogeneous calorimeter with 27 radiation lengths (r.l.) and 1.2 proton interaction lengths. The CR particle direction is reconstructed by IMC, made of 16 layers of thin scintillating fibers read out individually. The charge is identified by the CHD from Z = 1 to Z = 40 with excellent charge resolution. An independent charge measurement, via multiple samples of specific energy loss (dE/dx) in each fiber is also provided by IMC up to the onset of saturation which occurs for ions more highly charged than silicon.

CALET was launched on August 19, 2015 by the Japanese rocket H-II Transfer Vehicle (HTV-5) and installed on the Japanese Experiment Module Exposure Facility of the ISS. The on-orbit commissioning phase was successfully completed in the first days of October 2015. Calibration and test of the instrument took place at the CERN-SPS during five campaigns between 2010 and 2015 with beams of electrons, protons, and relativistic ions [25–27].

3. Data analysis

A period of 1613 days of flight data (FD) were analyzed for the present analysis. The total observation live time for the high-energy (HE) shower trigger is $T \sim 3.3 \times 10^4 h$, corresponding to 85.8% of total observation time. Energy calibration of each channel of CHD, IMC and TASC is performed by using penetrating proton and He particles, selected in-flight by a dedicated trigger mode. Raw signals are corrected for non-uniformity in light output, gain differences among

the channels, position and temperature dependence as well as temporal gain variations. After calibration, a track is reconstructed for each CR particle and each event is provided with an associated estimate of its charge and an energy. Detailed Monte Carlo (MC) simulations were developed, based on the EPICS package [28, 29] which implements the hadronic interaction model DPMJET-III [30]. The simulations are used to validate and tune the reconstruction method and evaluate event reconstruction efficiencies, background contaminations and the energy response matrix. An independent analysis based on FLUKA [31] is also performed to assess the systematic uncertainties. The incident CR track is found and fitted by a tracking algorithm based on a combinatorial Kalman filter fed with the coordinates provided by the scintillating fibers in the IMC. An angular resolution of ∼ 0.08° is found for iron nuclei. The resolution of the impact point on CHD is ∼ 180 μm. Events with a well-fitted primary track crossing the detector from CHD top to TASC bottom (and clear from the edges of TASCX1 and of the bottom TASC layer by at least 2 cm) are used in this analysis. The fiducial geometrical factor for this category of events is $S\Omega \sim 416\ cm^2 sr$, corresponding to about 40% of CALET total acceptance. In this analysis the onboard HE shower trigger, based on the coincidence of the summed dynode signals of the last four IMC layers and the top TASC layer (TASCX1) is used. Since the HE trigger is fully efficient (close to 100%) for elements heavier than oxygen an off-line trigger confirmation, as required for the analysis of lower charge elements [7, 12], is not necessary for iron. However, in order to select interacting particles, a deposit larger (2 sigmas) than the minimum ionization particle (MIP) peak is required in at least one of the first four layers of the TASC.

3.1 Charge identification

The identification of the charge Z is based on specific ionization *dE/dx* in CHD paddles traversed by the incident particle. Either CHD layer provides an independent *dE/dx* measurement. Corrections for the quenching effect in scintillator, due to high ionization density around the particle track, are applied based on fits of halo model to CALET data as a function of Z^2. The resulting curves are then used to reconstruct a charge value in either layer (Z_{CHDX}, Z_{CHDY}) on an event-by-event basis [12]. The systematic displacement of the CHDX and CHDY charge peaks to higher values with respect to the nominal charge position, due to an increasing amount of backscatters from the TASC at higher energy, is corrected by an energy dependent charge correction applied separately to the FD and the MC data. A charge distribution obtained by averaging Z_{CHDX} and Z_{CHDY} is shown in Fig.1. The CHD charge resolution σ_Z for iron is ∼ 0.35 (charge units). Residual background due to charge-changing nuclear interactions occurring in the upper part of the instrument are removed by requiring that the difference between the charges from either layer of the CHD is less than 1.5 charge units. Iron candidates are identified by an ellipse centered at Z = 26, with $1.25\sigma_x$ and $1.25\sigma_y$ wide semiaxes for Z_{CHDX} and Z_{CHDY}, respectively, and rotated clockwise by 45° as shown in the cross plot of the CHDY vs CHDX charge in Fig. 2.

3.2 Energy measurement

The shower energy E_{TASC} of each event is calculated as the sum of the calibrated energy deposits of all the TASC logs [32]. The simulated energy response was validated and tuned with beam test data, taken at CERN SPS in 2015 [25] using a beam of accelerated ion fragments with
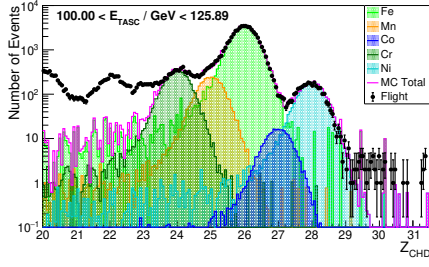
Figure 1: Charge distributions from the combined charge measurement of the two CHD layers. Flight data, represented by black dots, are compared with Monte Carlo samples including chromium, manganese, iron, cobalt and nickel.
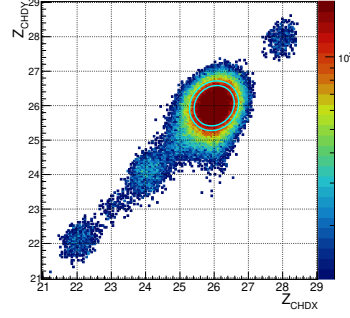

Figure 2: Crossplot of Z CHDY vs. Z CHDX reconstructed charges.The maximum and the minimum elliptical selection for the iron candidates are indicated by the cyan ellipses in the figure.

kinetic energy of 13,19 and 150 GeV/c/n. [12]. The energy response of the TASC is linear up to the maximum available particle energy of $\sim 6 TeV$ (obtained with a primary beam of ^{40}Ar nuclei); the fraction of particle energy released in the TASC is $\sim 20\%$. The energy resolution is $\sim 30\%$. Correction factors are 6.7% for $E_{TASC} < 45 GeV$ and 3.5% for $E_{TASC} > 350 GeV$, respectively. A linear interpolation is applied to determine the correction factor for intermediate energies. For nuclei with $Z > 10$, the TASC crystals undergo a light quenching phenomenon which is not reproduced by the MC simulations. Therefore, it is necessary to extract from the data a quenching correction to be applied *a posteriori* to the MC energy deposits generated in the TASC logs by noninteracting primary particles [33]. Distributions of E_{TASC} for iron candidate events selected in this analysis are shown in Fig. 3, together with the background expected from other nuclei mis-identified as iron. It can be noticed that the total background in the selected Fe event samples is negligible: $< 1\%$ in the energy range between 10^2 GeV and 10^3 GeV of E_{TASC} increasing up to $\sim 2\%$ at $E_{TASC} \sim 10^4$ GeV.
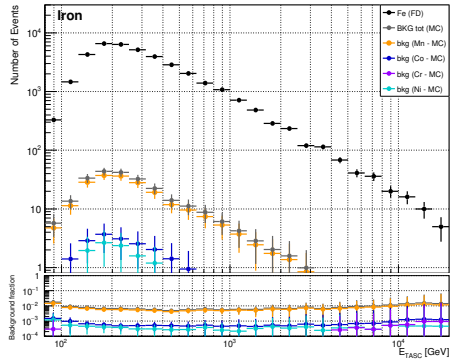

Figure 3: Top panel: Distribution of the total energy deposited in TASC by the selected iron nuclei in FD (black dots) before the unfolding procedure and with background events from nuclei close to iron in atomic number. Bottom panel: Contamination from each nuclear species between Z = 24 and Z = 28 from the MC.
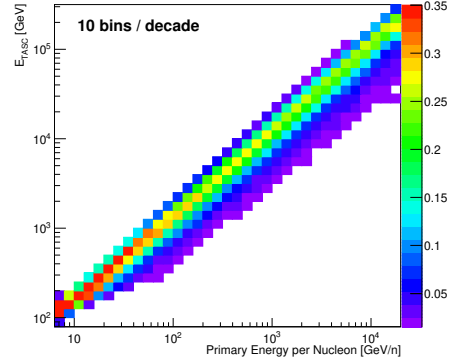

Figure 4: Response matrix for iron derived from the MC simulations of the CALET flight model by applying the same selection as for FD. The array is normalized so that the color scale is associated to the probability that iron candidates in a given bin of particle kinetic energy cover different intervals of E_{TASC}.

The energy released in TASC by hadrons is only a fraction of the primary particle energy. For flux measurement, energy unfolding is applied to correct E_{TASC} distributions for bin-to-bin migration effects (due to the limited energy resolution) and infer the primary particle energy. In this

analysis, we used the Bayesian approach [34] implemented within the RooUnfold package [35]. The response matrix, each element of which represents the probability that primary nuclei in a certain energy interval of the CR spectrum produce an energy deposit in a given E_{TASC} bin, is derived using MC simulation after applying the same selection procedure as for FD as shown in Fig.4.

4. Systematics errors

Fig. 5 shows a breakdown of energy dependent systematic errors stemming from several sources and including charge identification (1), MC model (2), energy scale correction (3), energy unfolding (4), beam test configuration (5) and shower event shape (6).
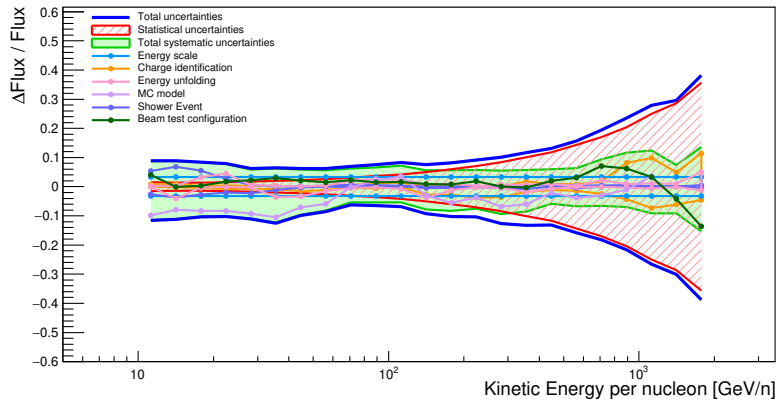

Figure 5: Energy dependence (in GeV/nucleon) of systematic uncertainties (relative errors) for iron. The band bounded by the red lines represents the statistical error. The shaded band within the green lines shows the sum in quadrature of all the sources of systematics including energy independent ones. The blue lines represent the sum in quadrature of statistical and total systematic uncertainties.

The systematic error related to charge identification (1) was studied by varying the semiaxes of the elliptical selection resulting a flux variation lower than a few percent below 600 GeV/n. Using FLUKA instead of EPICS simulation (2) the resulting in fluxes show a maximum discrepancy around 10% below 40 GeV/n. The uncertainty on the energy scale correction (3) is $\pm 2\%$ and causes a rigid shift of the measured energies, affecting the absolute flux normalization by $^{+3.3\%}_{-3.2\%}$, but not the spectral shape. The uncertainties due to the unfolding procedure (4) were evaluated with different response matrices computed by varying the spectral index (between -2.9 and -2.2) of the MC generation spectrum, or by using the Singular Value Deconvolution method, instead of the Bayesian approach. The contributions due to the beam test model (not identical to the instrument now in orbit) (5) and shower event cut (6) were evaluated and included in the systematic uncertainties. The systematic uncertainty due to off-acceptance events, tracking efficiency, background contamination and HE trigger efficiency are negligible. Energy-independent systematic uncertainties affecting the flux normalization include live time (3.4%), long-term stability (< 2%), and geometrical factor ($\sim 1.6\%$). The total systematic error is computed as the quadrature sum of all the sources of systematics in each energy bin.

5. Flux measurement

Fig. 6 shows the iron spectrum obtained with CALET. In comparison with other recent experiments, CALET iron spectrum is consistent with ATIC 02 [36] and TRACER [37] at low
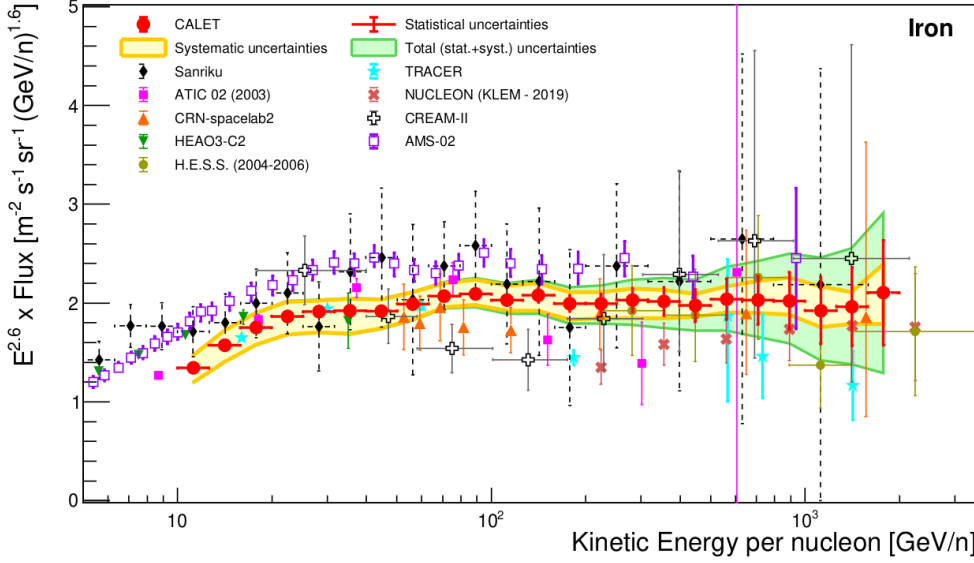
Figure 6: CALET iron flux (multiplied by $E^{2.6}$) as a function of kinetic energy per nucleon. Error bars of the CALET data (red) represent the statistical uncertainty only, the yellow band indicates the quadrature sum of systematic errors, while the green band indicates the quadrature sum of statistical and systematic errors. Also plotted are other direct measurements [36–44].

energy and with CRN [43] and HESS [41] at high energy, but differs in the absolute normalization with NUCLEON (lower) and Sanriku [40] (higher). CALET and AMS-02 [44] iron spectra have a very similar shape and comparable errors, but differ in the absolute normalization of the flux by ∼ 20% as shown in Fig. 7.
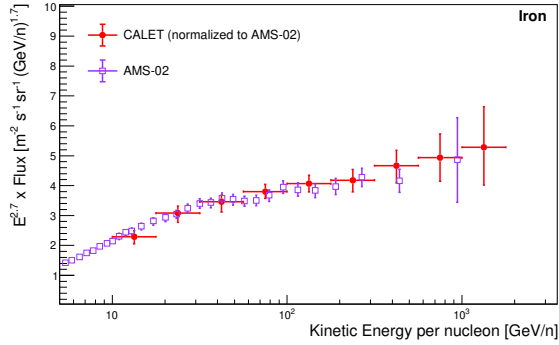

Figure 7: Iron flux (with multiplicative factor $E^{2.7}$) measured by CALET (red points) with 4 bins/decade, multiplied by 1.20 for comparison with the AMS-02 results [44]. The error bars of CALET data are the quadrature sum of statistical and systematic uncertainties.

Fig. 8 shows a fit to the CALET iron flux with a single power law (SPL) function from 50 GeV/n to 2.0 TeV/n. The fit gives a spectral index $\gamma = -2.60 \pm 0.02(stat) \pm 0.02(sys)$ with $\chi^2/DOF = 4.2/14$. The result is stable when the binning is changed from 10 to 4 bins/decade ($\gamma = -2.59 \pm 0.02(stat) \pm 0.04(sys)$). The spectral index γ is also calculated by a fit of $d[log(\Phi)]/d[log(E)]$ inside a sliding window centered in each energy bin and including the neighboring ±3 bins, in the region between 50 GeV/n and 2 TeV/n. The result in Fig. 9 shows that the iron flux, in the fit region, is compatible within the errors with a single power law.
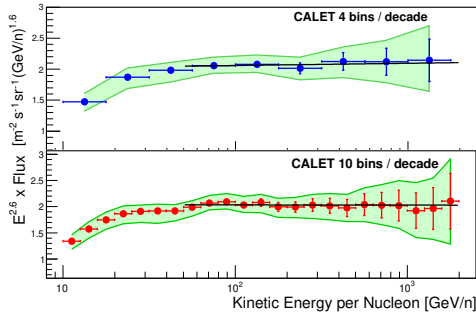
6

Figure 8: Fit of the CALET iron energy spectrum to a SPL function (black lines) in the energy range [50, 2000] GeV/n with 4 bins/decade (top) and 10 bins/decade (bottom).The green band indicates the quadrature sum of statistical and systematic errors.
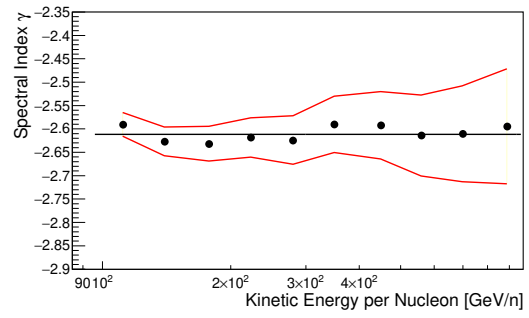

Figure 9: Energy dependence of the spectral index calculated within a sliding energy window for the CALET iron data.The fit with a constant function gives a mean spectral index value $\langle \gamma \rangle = -2.61 \pm 0.01$.

6. Conclusion

We report a measurement of the energy spectrum of iron from 10 GeV/n to 2.0 TeV/n with a significantly better precision than most of the existing measurements. Between 50 GeV/n and 2TeV/n our spectrum is consistent with the hypothesis of a SPL with a spectral index $\gamma = -2.60 \pm 0.03$. Beyond this energy limit, the uncertainties given by our present statistics and large systematics do not allow us to draw a significant conclusion on a possible deviation from a single power law.

References

[1] M. Aguilar et al. *Phys. Rev. Lett.* **114** (2015) 171103.

[2] M. Aguilar et al. *Phys. Rev. Lett.* **115** (2015) 211101.

[3] O. Adriani et al. *Science* **332** (2011) 69.

[4] Y.S. Yoon et al. *Astrophys. J.* **722** (2011) 122.

[5] Y.S. Yoon et al. *Astrophys. J.* **839** (2017) 5.

[6] Q. An et al. *Sci. Adv.* **5** (2019) eaax3793.

[7] O. Adriani et al. *Phys. Rev. Lett.* **122** (2019) 181102.

[8] M. Aguilar et al. *Phys. Rev. Lett.* **119** (2017) 251101.

[9] M. Aguilar et al. *Phys. Rev. Lett.* **120** (2018) 021101.

[10] M. Aguilar et al. *Phys. Rev. Lett.* **124** (2020) 211102.

[11] H.S. Ahn et al. *Astrophys. J. Lett.* **714** (2010) L89.

[12] O. Adriani et al. *Phys. Rev. Lett.* **125** (2020) 251102.

[13] P. Serpico in *Proceedings of Science (ICRC2015) 009*, 2015.

[14] N. Tomassetti *Astrophys. J. Lett.* **752** (2012) L13.

[15] P. Blasi et al. *Phys. Rev. Lett.* **109** (2012) 061101.

[16] C. Evoli et al. *Phys. Rev. D* **99** (2019) 103023.

[17] Y. Ohira et al. *Phys. Rev. D* **93** (2016) 083001.

[18] A. Vladimirov et al. *Astrophys. J.* **752** (2012) 68.

[19] S. Thoudam and J.R. Hörandel *Astron. Astrophys.* **567** (2014) A33.

[20] S. Torii and P.S. Marrocchesi *Adv. Space Res.* **64** (2019) 2531.

[21] S. Torii in *Proceedings of Science (ICRC2017) 1092*, 2017.

[22] Y. Asaoka in *Proceedings of Science (ICRC2019) 001*, 2019.

[23] O. Adriani et al. *Phys. Rev. Lett.* **119** (2017) 181101.

[24] O. Adriani et al. *Phys. Rev. Lett.* **120** (2018) 261102.

[25] Y. Akaike in *Proceedings of Science (ICRC2015) 613*, 2015.

[26] G. Bigongiari in *Proceedings of Science (ICRC2015) 592*, 2015.

[27] T. Niita et al. *Adv. Space Res.* **55** (2015) 2500.

[28] K. Kasahara in *Proc. of 24th ICRC*, vol. 1, p. 399, 1995.

[29] See EPICS webpage `http://cosmos.n.kanagawa-u.ac.jp/EPICSHome/`.

[30] S. Roesler et al. in *Proceedings of the Monte Carlo Conference, Lisbon, 1033-1038*, 2000.

[31] T.T. Böhlen et al. *Nuclear Data Sheets* **120** (2014) 211.

[32] Y. Asaoka et al. *Astroparticle Physics* **91** (2017) 1.

[33] O. Adriani et al. *Phys. Rev. Lett.* **126** (2021) 241101.

[34] G. D'Agostini *Nucl. Instr. and Meth. A* **362** (1995) 487.

[35] T. Adye in *Proc. of the PHYSTAT, CERN-2011-006*, 2011 [`arXiv:1105.1160`].

[36] A. Panov et al. *Bull. Russian Acad. Sci.* **73** (2009) 564.

[37] M. Ave et al. *Astrophys. J.* **678** (2008) 262–273.

[38] H.S. Ahn et al. *Astrophys. J.* **707** (2009) 593.

[39] V. Grebenyuk et al. *Adv. in Space Res.* **64** (2019) 2546.

[40] M. Ichimura et al. *Phys. Rev. D* **48** (1993) 1949.

[41] F. Aharonian et al. *Phys. Rev. D* **75** (2007) 042004.

[42] J.J. Engelmann et al. *Astron. Astrophys.* **233** (1990) 96.

[43] D. Müller et al. *Astrophys. J.* **374** (1991) 356.

[44] M. Aguilar et al. *Phys. Rev. Lett.* **126** (2021) 041104.

Full Authors List: CALET Collaboration

O. Adriani[1,2], Y. Akaike[3,4], K. Asano[5], Y. Asaoka[5], E. Berti[1,2], G. Bigongiari[6,7], W. R. Binns[8], M. Bongi[1,2], P. Brogi[6,7], A. Bruno[9,10], J. H. Buckley[8], N. Cannady[11,12,13], G. Castellini[14], C. Checchia[6], M. L. Cherry[15], G. Collazuol[16,17], K. Ebisawa[18], A. W. Ficklin[15], H. Fuke[18], S. Gonzi[1,2], T. G. Guzik[15], T. Hams[11], K. Hibino[19], M. Ichimura[20], K. Ioka[21], W. Ishizaki[5], M. H. Israel[8], K. Kasahara[22], J. Kataoka[23], R. Kataoka[24], Y. Katayose[25], C. Kato[26], N. Kawanaka[27,28], Y. Kawakubo[15], K. Kobayashi[3,4], K. Kohri[29], H. S. Krawczynski[8], J. F. Krizmanic[11,12,13], P. Maestro[6,7], P. S. Marrocchesi[6,7], A. M. Messineo[30,7], J.W. Mitchell[12], S. Miyake[32], A. A. Moiseev[33,12,13], M. Mori[34], N. Mori[2], H. M. Motz[35], K. Munakata[26], S. Nakahira[18], J. Nishimura[18], G. A. de Nolfo[9], S. Okuno[19], J. F. Ormes[36], N. Ospina[16,17], S. Ozawa[37], L. Pacini[1,14,2], P. Papini[2], B. F. Rauch[8], S. B. Ricciarini[14,2], K. Sakai[11,12,13], T. Sakamoto[38], M. Sasaki[33,12,13], Y. Shimizu[19], A. Shiomi[39], P. Spillantini[1], F. Stolzi[6,7], S. Sugita[38], A. Sulaj[6,7], M. Takita[5], T. Tamura[19], T. Terasawa[40], S. Torii[3], Y. Tsunesada[41], Y. Uchihori[42], E. Vannuccini[2], J. P. Wefel[15], K. Yamaoka[43], S. Yanagita[44], A. Yoshida[38], K. Yoshida[22], and W. V. Zober[8]

[1]Department of Physics, University of Florence, Via Sansone, 1, 50019 Sesto, Fiorentino, Italy, [2]INFN Sezione di Florence, Via Sansone, 1, 50019 Sesto, Fiorentino, Italy, [3]Waseda Research Institute for Science and Engineering, Waseda University, 17 Kikuicho, Shinjuku, Tokyo 162-0044, Japan, [4]JEM Utilization Center, Human Spaceflight Technology Directorate, Japan Aerospace Exploration Agency, 2-1-1 Sengen, Tsukuba, Ibaraki 305-8505, Japan, [5]Institute for Cosmic Ray Research, The University of Tokyo, 5-1-5 Kashiwa-no-Ha, Kashiwa, Chiba 277-8582, Japan, [6]Department of Physical Sciences, Earth and Environment, University of Siena, via Roma 56, 53100 Siena, Italy, [7]INFN Sezione di Pisa, Polo Fibonacci, Largo B. Pontecorvo, 3, 56127 Pisa, Italy, [8]Department of Physics and McDonnell Center for the Space Sciences, Washington University, One Brookings Drive, St. Louis, Missouri 63130-4899, USA, [9]Heliospheric Physics Laboratory, NASA/GSFC, Greenbelt, Maryland 20771, USA, [10]Department of Physics, Catholic University of America, Washington, DC 20064, USA, [11]Center for Space Sciences and Technology, University of Maryland, Baltimore County, 1000 Hilltop Circle, Baltimore, Maryland 21250, USA, [12]Astroparticle Physics Laboratory, NASA/GSFC, Greenbelt, Maryland 20771, USA, [13]Center for Research and Exploration in Space Sciences and Technology, NASA/GSFC, Greenbelt, Maryland 20771, USA, [14]Institute of Applied Physics (IFAC), National Research Council (CNR), Via Madonna del Piano, 10, 50019 Sesto, Fiorentino, Italy, [15]Department of Physics and Astronomy, Louisiana State University, 202 Nicholson Hall, Baton Rouge, Louisiana 70803, USA, [16]Department of Physics and Astronomy, University of Padova, Via Marzolo, 8, 35131 Padova, Italy, [17]INFN Sezione di Padova, Via Marzolo, 8, 35131 Padova, Italy, [18]Institute of Space and Astronautical Science, Japan Aerospace Exploration Agency, 3-1-1 Yoshinodai, Chuo, Sagamihara, Kanagawa 252-5210, Japan, [19]Kanagawa University, 3-27-1 Rokkakubashi, Kanagawa, Yokohama, Kanagawa 221-8686, Japan, [20]Faculty of Science and Technology, Graduate School of Science and Technology,, Hirosaki University, 3, Bunkyo, Hirosaki, Aomori 036-8561, Japan, [21]Yukawa Institute for Theoretical Physics, Kyoto University, Kitashirakawa Oiwakecho, Sakyo, Kyoto 606-8502, Japan, [22]Department of Electronic Information Systems, Shibaura Institute of Technology, 307 Fukasaku, Minuma, Saitama 337-8570, Japan, [23]School of Advanced Science and Engineering, Waseda University, 3-4-1 Okubo, Shinjuku, Tokyo 169-8555, Japan, [24]National Institute of Polar Research, 10-3, Midori-cho, Tachikawa, Tokyo 190-8518, Japan, [25]Faculty of Engineering, Division of Intelligent Systems Engineering, Yokohama National University, 79-5 Tokiwadai, Hodogaya, Yokohama 240-8501, Japan, [26]Faculty of Science, Shinshu University, 3-1-1 Asahi, Matsumoto, Nagano 390-8621, Japan, [27]Hakubi Center, Kyoto University, Yoshida Honmachi, Sakyo-ku, Kyoto 606-8501, Japan, [28]Department of Astronomy, Graduate School of Science, Kyoto University, Kitashirakawa Oiwake-cho, Sakyo-ku, Kyoto 606-8502, Japan, [29]Institute of Particle and Nuclear Studies, High Energy Accelerator Research Organization, 1-1 Oho, Tsukuba, Ibaraki 305-0801, Japan, [30]University of Pisa, Polo Fibonacci, Largo B. Pontecorvo, 3, 56127 Pisa, Italy, [31]Astroparticle Physics Laboratory, NASA/GSFC, Greenbelt, Maryland 20771, USA, [32]Department of Electrical and Electronic Systems Engineering, National Institute of Technology, Ibaraki College, 866 Nakane, Hitachinaka, Ibaraki 312-8508, Japan, [33]Department of Astronomy, University of Maryland, College Park, Maryland 20742, USA, [34]Department of Physical Sciences, College of Science and Engineering, Ritsumeikan University, Shiga 525-8577, Japan, [35]Faculty of Science and Engineering, Global Center for Science and Engineering, Waseda University, 3-4-1 Okubo, Shinjuku, Tokyo 169-8555, Japan, [36]Department of Physics and Astronomy, University of Denver, Physics Building, Room 211, 2112 East Wesley Avenue, Denver, Colorado 80208-6900, USA, [37]Quantum ICT Advanced Development Center, National Institute of Information and Communications Technology, 4-2-1 Nukui-Kitamachi, Koganei, Tokyo 184-8795, Japan, [38]College of Science and Engineering, Department of Physics and Mathematics, Aoyama Gakuin University, 5-10-1 Fuchinobe, Chuo, Sagamihara, Kanagawa 252-5258, Japan, [39]College of Industrial Technology, Nihon University, 1-2-1 Izumi, Narashino, Chiba 275-8575, Japan [40]RIKEN, 2-1 Hirosawa, Wako, Saitama 351-0198, Japan, [41]Division of Mathematics and Physics, Graduate School of Science, Osaka City University, 3-3-138 Sugimoto, Sumiyoshi, Osaka 558-8585, Japan, [42]National Institutes for Quantum and Radiation Science and Technology, 4-9-1 Anagawa, Inage, Chiba 263-8555, Japan, [43]Nagoya University, Furo, Chikusa, Nagoya 464-8601, Japan, [44]College of Science, Ibaraki University, 2-1-1 Bunkyo, Mito, Ibaraki 310-8512, Japan